# Load-Dependent Composite Action for Beam Nonlinear and Ductile Behavior

Yu Bai, Ph.D.[1]; and Chengyu Qiu[2]

**Abstract:** Ductile performance of beam structures often is achieved by material yielding or progressive failure of components. A new structural concept was developed and validated in this study to provide ductile responses of beam structures through load-dependent composite action resulting from the change in the modulus of shear connection. Layered beam specimens made from linear elastic fiber-reinforced polymer (FRP) members shear-connected by a nonlinear elastoplastic adhesive were tested to demonstrate this concept. Evidenced by the shear slip between the beam layers and the section strain distribution, the decrease in beam stiffness and thus the ductile load-displacement response originates from the reduced composite action between the beam layers. Recovery of the beam residual deformation after unloading occurred because of the nonlinear elastoplastic behavior of the adhesive. Finite-element (FE) modeling was conducted and well described the ductile load-displacement response and the change in composite action. Parametric studies were carried out to clarify the effects of adhesive modulus and strength on the load-dependent composite action and overall ductile performance. FE modeling was conducted to demonstrate the applicability of the concept for further engineering practice. **DOI: 10.1061/(ASCE)ST.1943-541X.0002563.**


**Author keywords:** Nonlinear deformation; Ductility; Load-dependent composite action; Composite beam; Ductile adhesive; Shear connection.



## Introduction

The ability of a structure to undergo large nonlinear deformation without loss of load-carrying capacity, which also is referred to as ductility (if energy dissipation is involved), is preferred because of the potential to provide warning prior to structural failure. In most cases, this structural performance is realized by material ductility. Thus steel, for example, commonly has been used, either alone or as the reinforcement in concrete. Many other materials may provide new options in structural construction, such as glasses because of their transparency and aesthetic appearance [C. Deminet, R. B. Gillette, "All glass composite building panels," US Patent No. 3,981,294 (1976)]; timbers because of their low energy of production and recyclability (Dodoo et al. 2014); and bamboos because of their excellent longitudinal strength, good flexibility (Amada et al. 1997), and speed of growth (Liese 1987). Among these, fiber-reinforced polymer (FRP) composites have attracted interest as lightweight corrosion-resistant materials that are as strong as steels in the fiber direction (Hollaway 2010). Nevertheless, widespread structural application of these materials is impeded by their inherent lack of material ductility. With these linear elastic and brittle materials, designers must consider relatively large safety factors (Chambers 1997; Porteous and Kermani 2013) or resort to other means to achieve nonlinear load-deformation responses at the structural level.

Ductile behavior at the structural level can be realized by proper combinations of ductile and brittle materials, for example, steel-reinforced concrete. Another successful example was steel–concrete composite beams (Chapman and Balakrishnan 1964) in which the steel section was designed to develop its yielding capacity before crushing of the top concrete flange. This methodology subsequently was implemented in hybrid beams consisting of a FRP cellular deck bonded onto a steel girder (Keller and Gürtler 2005; Satasivam and Bai 2016). For FRP members with square hollow sections, beam–column (Zhang et al. 2018) and column splice connections (Qiu et al. 2018) were proposed that utilized yielding in the steel bolted flange joint component to achieve ductile performance. Ductile FRP adhesive lap joints were demonstrated using a ductile acrylic adhesive (de Castro and Keller 2008). With this adhesive, double strap joints were developed to splice FRP beams, forming plastic hinges upon bending to redistribute the internal forces in a redundant system (Keller and de Castro 2005).

For linear elastic and brittle materials, attempts were made to achieve a nonlinear load-deformation response using the concept of pseudoductility, that is, exploiting the progressive failure of brittle components in a redundant system. In FRP and hybrid structures, a hybrid beam was proposed, consisting of a pultruded glass FRP (GFRP) box-section beam with a concrete block on top and a carbon FRP (CFRP) plate bonded at the bottom (Meier et al. 1995). Pseudoductile behavior was demonstrated by the progressive failure of the CFRP plate fracturing followed by concrete crushing. In another hybrid concrete-FRP beam design, pseudo-ductile failure was realized through the development of a series of tensile and shear cracks in the lightweight concrete core (Keller et al. 2007). Pseudoductile failure also was achieved in a series of concrete–FRP composite slabs through the progressive failure in the FRP dowel shear connectors (Gai et al. 2013). Further examples of pseudoductile FRPs and hybrid structures through progressive failure were discussed by Bank (2012). The concept of pseudoductility also was employed to improve the postelastic robustness of timber structures. Glue-laminated timber beams were assembled with lamellae of

[1]Professor, Dept. of Civil Engineering, Monash Univ., Clayton, VIC 3800, Australia. Email: yu.bai@monash.edu

[2]Postgraduate Student, Dept. of Civil Engineering, Monash Univ., Clayton, VIC 3800, Australia (corresponding author). Email: chengyu.qiu@monash.edu

Note. This manuscript was submitted on February 18, 2019; approved on September 3, 2019; published online on January 27, 2020. Discussion period open until June 27, 2020; separate discussions must be submitted for individual papers. This paper is part of the ***Journal of Structural Engineering***, © ASCE, ISSN 0733-9445.

different grades (Tomasi et al. 2009). Considerable postelastic deformation was reported, caused by the progressive rupture of different lamellae. Another strategy proposed recently realized reversible nonlinear deformation utilizing the elastic buckling of certain compressive members in a truss structure (Bai and Zhang 2012). Demonstrated by planar trusses assembled of brittle FRP members, the concept was further implemented in large-scale spatial trusses under static (Yang et al. 2015) and dynamic and fatigue loading (Yang et al. 2016).

Unlike the aforementioned strategies, a new concept is proposed in this paper to realize nonlinear load-deformation responses and structural ductility in layered beam structures through changes in the degree of composite action during loading. The subject of composite action has been widely studied in the literature, such as that for steel–concrete composite beams (Culver and Coston 1961), timber–concrete composite beams (Clouston et al. 2005), and FRP–concrete composite beams (Correia et al. 2007). Despite the use of shear connectors, partial composite action and thus additional beam deformation can be caused by insufficient number of shear connectors and their deformability under shear loading (Nie and Cai 2003). To include the resulting partial composite action, analysis was conducted by considering the shear-slip behavior that could be characterized by push-out (Jayas and Hosain 1988; Steinberg et al. 2003) or pull shear tests (Satasivam et al. 2017) on shear connectors. The preceding studies noted that composite action and the resulting beam stiffness may decrease due to the softening between the two materials in composite beams. This softening behavior corresponded to the failure of shear connectors that may occur in a progressive manner or with sudden structural collapse (Nie et al. 2008). The effects of shear connectors on the composite beam performance also were investigated in the literature. Based on the secant stiffness of shear connectors, an analytical solution was developed by Wang (1998) to calculate the overall deflection of steel–concrete composite beams. Numerical studies were conducted to describe the mechanical responses of composite beams, taking into account the softening of shear connectors, i.e. their yielding, large deformation, or failure (Salari et al. 1998; Faella et al. 2003). It was further pointed out by Oehlers et al. (2013) that the ductility of RC is affected by, in addition to the yielding of steel reinforcements, the shear interaction and thus composite action between the concrete and reinforcements. In previous studies of steel–concrete composite beams and RC structures, the additional deformation caused by the reduced composite action between the steel and concrete was the inevitable consequence of interface softening (i.e. concrete damage around steel reinforcement) or failure of steel shear connectors as loading increased, rather than a designed response to provide structural ductility. This study proposes that, for general layered beam structures made of linear elastic and brittle materials, the change in composite action during loading can be actively used to introduce a decrease in flexural stiffness and therefore to provide structural ductility. Manipulation of the composite action can be realized by means of an elastoplastic ductile adhesive as a shear connection, in contrast to the progressive or brittle failure of shear connectors or interfaces in composite or RC beams.

The proposed concept is illustrated in Fig. 1 using a simple layered beam structure shear-connected by ductile adhesive. The ductile adhesive features an elastoplastic stress–strain relationship in shear and is available commercially with various stiffnesses and strengths, such as DP8005 (3M, Saint Paul, Minnesota), Hysol EA 9361 (Henkel, Düsseldorf, Germany), and Araldite 2021 (Huntsman, Monthey, Switzerland). Other types of shear connector with nonlinear stress–strain relationships also may be considered for this purpose. Under flexural loading, initially (Fig. 1, Stage 1) the shear connection (the adhesive layer, for example) has high

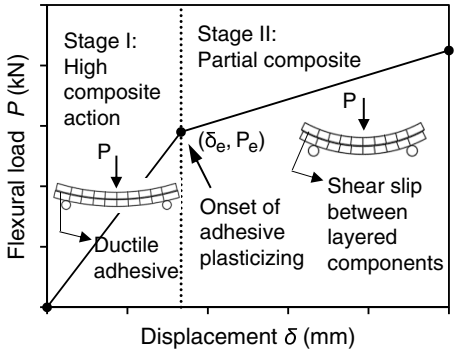


**Fig. 1.** Design concept for realizing nonlinear load-deformation response in beam structures.

shear stiffness and therefore provides high (or full) composite action between the layered components of the beam. Beyond a certain load level, degradation of the composite action is induced by the decreased shear modulus of the adhesive (acting as shear connection). As a result, the beam structure deforms with reduced flexural stiffness and substantial shear slip between its layered components (Fig. 1, Stage 2), producing a nonlinear load-deformation response. The final failure may be governed by the material failure of the layered components or by the adhesive layer acting as shear connection; whereas the transition from Stage 1 to Stage 2, at which the elastic load $P_e$ can be defined, occurs when the adhesive layer begins its plasticization (i.e., with a significant decrease in its shear modulus) and thus no longer is able to maintain the high composite action of Stage 1. This structural concept, illustrated here with a beam configuration, can be applied to other layered structures made of linear elastic and brittle materials, such as sandwich structures (Manalo et al. 2010; Keller et al. 2014; Satasivam et al. 2014), built-up section beams (Hejll et al. 2005; Bai et al. 2013), or composite beams (Nordin and Täljsten 2004; Correia et al. 2007) to realize ductile structural failure if the shear connection is properly designed to introduce reduced composite action with load increase before the ultimate failure.

To demonstrate this structural concept, experimental investigations were designed and conducted on layered beam specimens made of brittle FRP material and a ductile adhesive. Specimens with a linear elastic adhesive also were tested for reference. Strain responses were recorded to demonstrate the development of partial composite action. In addition to the scenario of monotonic loading, the behaviors of the layered beam specimens (with linear or ductile adhesive) were further explored under load–unload–reload cycles. Finite-element (FE) modeling was performed, not only to predict the nonlinear load-deformation responses but also to assess the effect of adhesive strength and modulus on the beam performance.

## Experimental Program

### *Specimens*

Layered beam specimens were prepared by bonding together two rectangular-section FRP beams with adhesive. Configuration and dimensions of the specimens are illustrated in Fig. 2. The bonded surfaces of the FRP were abraded with 180-grit sanding sheet and cleaned with acetone before application of the adhesive. Two types of adhesive were used: a linear elastic epoxy-based adhesive, or a nonlinear elastoplastic acrylic-based adhesive. The thickness of the adhesive layer was controlled using 0.5-mm-diameter spacers

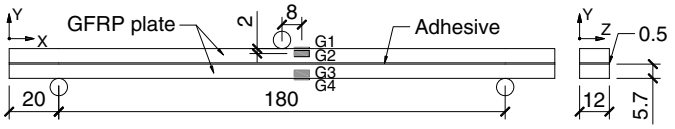


**Fig. 2.** Dimensions and strain gauge positioning of the layered beam specimens (unit: millimeters).

between the two FRP beams. The assembled specimens were cured at room temperature for 7 days (specimens with epoxy adhesive) or 3 days (specimens with acrylic adhesive) before testing, in accordance with the manufacturers' recommendations. The design geometry was intended to have the decrease of adhesive shear modulus precede other nonlinear structural responses or damages, and thus clearly focus on the targeted reduction in composite action to demonstrate the proposed concept. Eight beam specimens were prepared for the subsequent three-point bending tests (Table 1). The first letter (E or A) of the specimen name refers to the type of adhesive used (epoxy or acrylic-based); the second letter (M or C) denotes the type of loading (monotonic or load–unload–reload cycles); and the number (1 or 2) indexes the duplicate specimens.

### Material Properties

The FRP rectangular sections were cut from a pultruded flat panel along the fiber direction. The pultruded FRP material consisted of E-glass fibers (47.8% by volume) embedded in polyester resin (Satasivam et al. 2014). The fiber architecture comprised one unidirectional roving layer between two mat layers. The strength and modulus properties of the FRP, obtained according to relevant standards and methods, are summarized in Table 2. The two two-component adhesives used were epoxy-based Sikadur-330 (Sika, Zug, Switzerland) and acrylic-based DP8005 (3M, Saint Paul, Minnesota). Tensile dog-bone samples of Sikadur-330 and DP8005 were tested by Qiu et al. (2019) and Pinto et al. (2009), respectively. The stress–strain behaviors and strength and modulus properties are presented in Fig. 3. The Sikadur-330 exhibited a linear stress–strain behavior up to failure, whereas the ductile adhesive DP8005 had linear behavior initially and then a considerable increase in strain with almost constant stress, based on which the plastic strength ($\sigma_p$) of DP8005 was defined.

### Instrumentation and Loading Program

This study adopted a three-point bending setup [Figs. 2 and 4(a)]. The flexural load ($P$) at midspan was applied by an Instron machine (Norwood, Massachusetts) with a 5-kN-capacity load cell. In each specimen, Strain gauges G1 to G4 (Fig. 2) were deployed along

**Table 2.** Strength and modulus of FRP material

| Orientation and component | Strength (MPa) | Modulus (GPa) | Method |
|---|---|---|---|
| Longitudinal tensile | $393.1 \pm 7.0$ | $31.7 \pm 0.7$ | ASTM D3039 (ASTM 2014) |
| Transverse tensile | $22.0 \pm 2.1$ | $5.0 \pm 0.2$ | ASTM D3039 (ASTM 2014) |
| In-plane shear | $20.8 \pm 1.4$ | $3.5 \pm 0.7$ | 10° off-axis tensile test (Lee et al. 1990) |

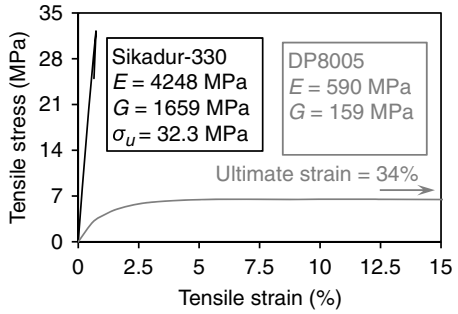


**Fig. 3.** Typical tensile stress-strain curves of adhesives Sikadur-330 and DP8005 and their material properties ($E$ = elastic modulus, $G$ = shear modulus, $\sigma_u$ = ultimate strength, and $\sigma_p$ = plastic strength).

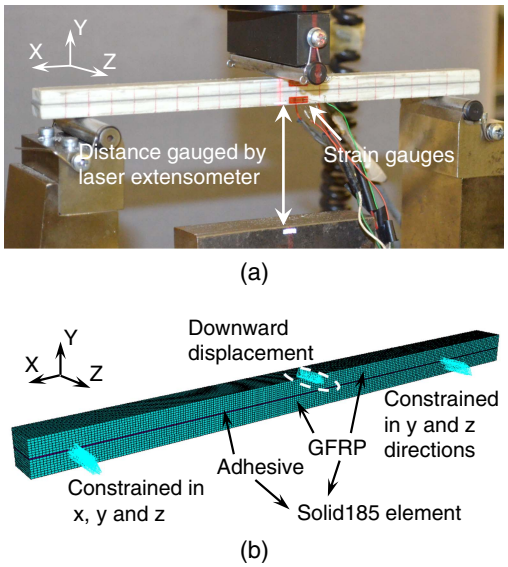


**Fig. 4.** Layered beam specimens under three-point bending: (a) experimental setup; and (b) FE modeling.

**Table 1.** Experimental and FE results for all layered beam specimens

| Specimen[a] | Initial stiffness[b] (kN/mm) | | | Elastic load[b,d] (kN) | | | Ultimate load[b] (kN) | | |
|---|---|---|---|---|---|---|---|---|---|
| | $S$ | $S_{FE}$[c] | $S/S_{FE}$ | $P_e$ | $P_{e,FE}$[c] | $P_e/P_{e,FE}$ | $P_u$ | $P_{u,FE}$[c] | $P_u/P_{u,FE}$ |
| EM-1 and EM-2 | 0.347 | 0.414 | 0.838 | — | — | — | 2.64 | 2.88 | 0.917 |
| AM-1 and AM-2 | 0.313 | 0.374 | 0.837 | 0.74 | 0.86 | 0.860 | 1.90 | 1.98 | 0.960 |
| EC-1 and EC-2 | 0.365 | — | — | — | — | — | 2.73 | — | — |
| AC-1 and AC-2 | 0.316 | — | — | 0.83 | — | — | 1.97 | — | — |

[a]E = epoxy adhesive; A = acrylic adhesive; M = monotonic loading; and C = load–unload–reload cyclic loading.
[b]Average value of two repeated specimens.
[c]Results from FE modeling.
[d]Intersection point of initial and postelastic tangent lines.

the depth of a cross section close to the midspan. Vertical displacement at the midspan ($\delta$) was measured by a laser extensometer [Fig. 4(a)]. In addition to monotonic loading (on Specimens EM-1, EM-2, AM-1, and AM-2), load–unload–reload cycles were applied (on Specimens EC-1, EC-2, AC-1, and AC-2). Unloading (to 0 kN) of the EC specimens occurred at 0.80 and 1.60 kN, corresponding to about 32% and 64% of their ultimate loads, respectively. The AC specimens were unloaded (to 0 kN) at three load levels, 0.20, 0.85, and 1.25 kN, the latter two of which were designed to occur at the nonlinear stage of the load-displacement response (Fig. 1, Stage 2).

The loading and unloading at midspan were applied with a crosshead speed of 1 mm/min. Considering the viscoelastoplastic behavior of the acrylic adhesive reported by de Castro and Keller (2008), after the unloading at 0.85 and 1.25 kN, the AC specimens were kept free of loading for about 3 and 18 h, respectively, and their recovery of deformation was gauged by the laser extensometer. All the cyclic loading programs were completed with a final reloading (after the 18-h recovery) until ultimate failure of the specimens.

## FE Modeling

FE modeling was conducted for the monotonically loaded specimens EM-1, EM-2, AM-1, and AM-2 using the ANSYS Mechanical APDL version 16.2 package. The load–unload–reload scenarios were not simulated because of the lack of reliable viscoelastoplastic material properties of the acrylic adhesive and because the time dependence of the adhesive deformation was not the focus of this study. The monotonic loading scenarios were sufficient to demonstrate the realization of nonlinear and ductile structural responses resulting from the load-dependent composite action. Three-dimensional (3D) models were constructed using 3D 8-node solid elements (SOLID185) [Fig. 4(b)]. Each FRP section was meshed into 8 elements through its thickness, 8 elements across its width, and 200 elements along the 180-mm-net span. The adhesive layer was divided into two elements through the thickness.

The FRP material was defined as orthotropic linear elastic with the modulus properties listed in Table 2. The epoxy adhesive Sikadur-330 was modeled as an isotropic linear elastic material with the elastic and shear moduli given in Fig. 3. Ward (1971) and Quinson et al. (1997) showed that under shear- or tension-dominant stress states, the yield stress of acrylic polymer materials can be described satisfactorily by the von Mises criterion. As the shear connection in the layered beams, the adhesive layer was mainly in shear. Therefore, the von Mises yield criterion with flow rule after yielding was adopted for the acrylic adhesive DP8005 in this study. Using an elastic-plastic bilinear stress–strain model, the elastic modulus and plastic strength of the acrylic adhesive were defined with the values obtained from tensile testing (Fig. 3). To model the simply supported boundary condition, the nodes of the specimens at the support locations were constrained in the $x$-, $y$-, and $z$-directions at one end, and in the $y$- and $z$-directions at the other end to allow elongation or shortening in the $x$-direction [Fig. 4(b)]. This modeling approach is typical practice for simply supported boundary condition as commonly used in the literature (Salari et al. 1998; Queiroz et al. 2007). Downward displacement was applied to the top nodes at midspan to simulate application of the flexural load. The mechanical responses of the beam structure under the aforementioned boundary conditions were solved in an incremental load step with 50 uniform increments using the Newton–Raphson method.

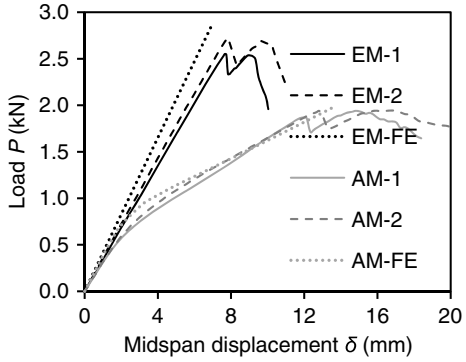


**Fig. 5.** Load-displacement ($P$-$\delta$) response of the beam specimens under monotonic loading.

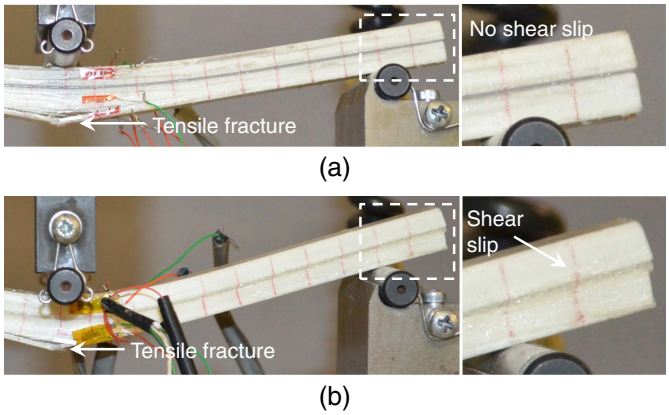


**Fig. 6.** Deformations and failure modes: (a) specimens with epoxy adhesive; and (b) specimens with acrylic adhesive.

## Results and Discussion

### *Load-Displacement Response and Failure Mode*

Fig. 5 presents the load-displacement ($P$-$\delta$) curves of the monotonically loaded specimens (EM-1, EM-2, AM-1, and AM-2). Specimens EM-1 and EM-2 exhibited linear $P$-$\delta$ responses up to an average ultimate load $P_u$ of 2.64 kN, at which tensile fracture of the FRP happened at the soffit of the specimens [Fig. 6(a)]. Specimens AM-1 and AM-2 successfully demonstrated a bilinear $P$-$\delta$ response as conceptualized in Fig. 1. Their $P$-$\delta$ curves developed initially with stiffness similar to that of EM-1 and EM-2, before a reduction in stiffness, which began at about 0.58 kN (Fig. 5). The reduction in stiffness is believed to be caused by the change in the shear modulus of the ductile acrylic adhesive under shear loading, leading to a decrease in the degree of composite action between the bonded FRP sections. This was further evidenced by the shear slip between the two FRP sections [Fig. 6(b)], in which the original cross section in a plane deformed into two separate sections that slid relative to each other due to the formation of their own neutral axes. The ultimate failure (at an average $P_u$ of 1.90 kN) of AM-1 and AM-2, in a similar mode as EM-1 and EM-2, occurred as tensile fracture of the FRP at the soffit [Fig. 6(b)].

Fig. 7 presents the $P$-$\delta$ curves of EC-1, EC-2, AC-1, and AC-2 under load–unload–reload cycles. Overall, the failure modes were identical to those of EM-1, EM-2, AC-1, and AC-2 (Fig. 6), and the envelopes of the cyclic $P$-$\delta$ curves resembled those of their

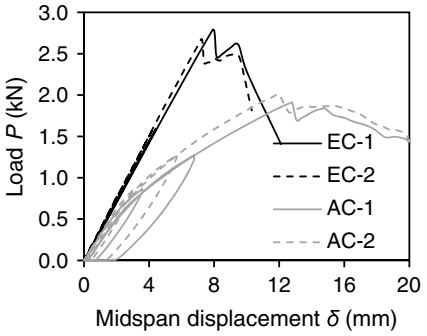


**Fig. 7.** Load-displacement ($P$-$\delta$) response of the beam specimens under load–unload–reload cycles.

monotonically loaded counterparts. The EC specimens, unloaded at 0.80 and 1.60 kN, showed that both unloading and reloading paths were linear and coincided with the initial loading path. The first unloading of the AC specimens occurred at 0.20 kN, which was within the linear stage of the $P$-$\delta$ curve, producing unloading and reloading responses that coincided with the initial loading path. The second and third unloadings occurred at 0.85 and 1.25 kN, respectively, beyond the linear stage. These two unloading paths were nonlinear and ended at 0 kN with a certain residual displacement (Fig. 7). Monitored for about 3 h after the unloading from 0.85 kN and 18 h after the unloading from 1.25 kN, the residual displacements were found to recover and converge to a threshold of about 80% recovery (with less than 0.5% change in the following 20 min). This time-dependent recovery of deformation is discussed in further detail in section "Recovery of Beam Deformation after Unloading." The subsequent reloading of AC-1 and AC-2 produced nonlinear $P$-$\delta$ responses with almost the same slopes as the initial loading paths (Fig. 7).

The stiffness and load capacities of all the specimens are summarized in Table 1. The specimens with acrylic adhesive (AM-1, AM-2, AC-1, and AC-2) exhibited 11.7% lower initial stiffness than the epoxy specimens (EM-1, EM-2, EC-1, and EC-2). The loading type (monotonic or cyclic) did not introduce a notable effect on the mechanical characteristics identified from the $P$-$\delta$ responses. For example, comparison of AM-1 and AM-2 with AC-1 and AC-2 shows that the elastic loads ($P_e$, the intersection point of the initial and postelastic tangent lines) were within 5.8%, and the ultimate loads ($P_u$) were within 1.9%. Fig. 5 plots the $P$-$\delta$ responses from FE modeling with the experimental responses for specimens EM-1, EM-2, AM-1, and AM-2. In the FE modeling, the ultimate load ($P_{u,FE}$) was deemed to be reached when the tensile strain at the soffit of the specimen reached the average peak strain of 1.73% measured in the experiments. For specimens AM-1 and AM-2, the FE modeling was able to capture the nonlinear $P$-$\delta$ response, predicting an elastic load, $P_{e,FE}$, of 0.86 kN (compared with the experimental value, $P_e$, of 0.74 kN, a difference of 15%). Table 1 compares the major results of the experiment and FE modeling. The slight overestimation of initial stiffness ($S$) and load capacities ($P_e$ and $P_u$) by the FE modeling may be due partly to the imperfect bond quality of the specimens.

### Composite Action between Two Bonded Sections

The strain measurements from G1 to G4 deployed along the section depth (Fig. 2) allow understanding of the composite action between the two bonded sections. Fig. 8 shows the strain distributions from the EM (with epoxy adhesive) and AM (with acrylic adhesive) specimens at different load levels. In EM-1 [Fig. 8(a)], the axial strains were distributed linearly along the depth of the section up to 100% of $P_u$, indicating full composite action between the bonded sections. In contrast, specimen AM-1 [Fig. 8(b)] had nonlinearity in the strain distribution along the section depth, for example, at 50% of $P_u$, and such nonlinearity became more significant as the load increased. The development of nonlinear strain distribution suggests that the original cross section with composite action was bent into two sections with different curvatures and neutral axes, echoing the shear slip between the two bonded sections observed in the AM and AC specimens [Fig. 6(b)].

The onset of the decrease in composite action was triggered when reduction of the stiffness of the shear connection occurred, i.e. when the adhesive layer was loaded into the plastic stage (Fig. 3) and thus became incapable of maintaining the initial high composite action at the early stage. The nonlinearity in the strain distribution, as an indication of the partial composite action, was found to match the stiffness reduction in the load-displacement ($P$-$\delta$) curves (Fig. 5). This further confirmed the realization of the design concept (Fig. 1). The strain distribution from FE modeling also is plotted in Fig. 8(b) for the AM specimen. Good agreement with the experimental results was obtained, such that the development of strain distribution with load levels was well described. This comparison verified that the nonlinear $P$-$\delta$ response from FE modeling stemmed from the same mechanism as that in the experimental specimens.

### Recovery of Beam Deformation after Unloading

A ductile acrylic adhesive (SikaFast550, Sika, Zug, Switzerland) was reported with time-dependent recovery of residual deformation after the removal of tensile loading (de Castro and Keller 2008). It therefore was expected that the specimens with acrylic adhesive in this study would exhibit similar behavior. To confirm this, after the

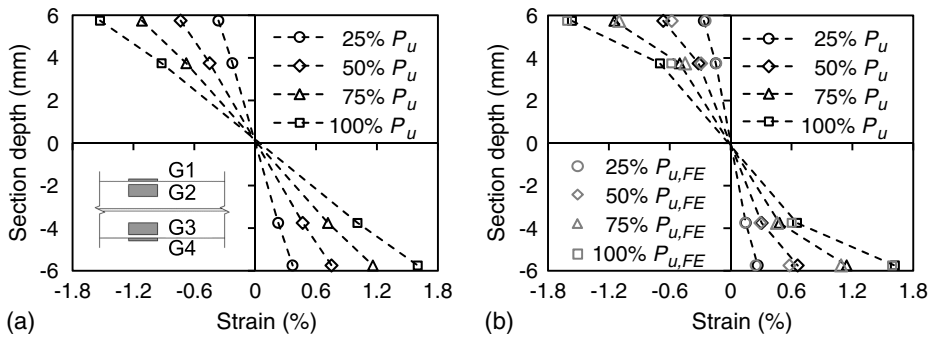


**Fig. 8.** Strain distribution along section depth: (a) Specimen EM-1; and (b) Specimen AM-1.

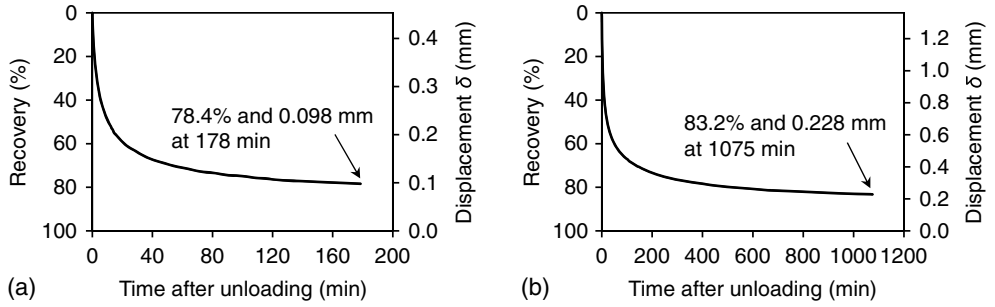


**Fig. 9.** Recovery of residual midspan displacement ($\delta$) with time (Specimen AC-2): (a) after unloading at 0.85 kN; and (b) after unloading at 1.25 kN.



**Table 3.** Ductile adhesives of different modulus and strength

| Adhesive | Chemical base | Elastic modulus (MPa) | Shear modulus (MPa) | Tensile strength (MPa) | Ultimate strain | References |
|---|---|---|---|---|---|---|
| Araldite 2021 | Toughened methacrylate | 1,130 | — | 26.2 | 0.40 | Banea and da Silva (2010) |
| Hysol EA 9361 | Epoxy | 670 | 239 | 8.0 | 0.44 | da Silva et al. (2008) |
| SikaFast-5211 | Acrylic | 260 | — | 5.1 | 0.47 | da Silva et al. (2006) |
| SikaFlex-552 | Silane-terminated polymer | 4.17 | 1.30 | 2.5 | 2.31 | Machado et al. (2018) |

unloading at 0.85 and 1.25 kN, the AC specimens were kept free of loading for a certain duration while the midspan displacement ($\delta$) was being gauged. Figs. 9(a and b) present the curves of midspan displacement $\delta$ versus the time after unloading for Specimen AC-2. Immediately after the complete unloading from 0.85 kN, a residual displacement of 0.453 mm remained [Fig. 9(a)]. This displacement quickly recovered 50% during the first 10.4 min but gradually slowed subsequently. The specimen eventually was reloaded at 178 min after the unloading, when the recovery barely progressed, approaching a plateau of about 78.4% of the initial residual displacement.

After the unloading from 1.25 kN, the recovery curve of specimen AC-2 exhibited a similar response [Fig. 9(b)]. The specimen recovered 50% in the first 20.9 min before it gradually stabilized and converged to a plateau of about 83.2% after 1,075 min. Because the FRP remained in the elastic range, the recovery of beam deformation suggested reversibility of the nonlinear shear deformation of the acrylic adhesive. Because this ductile adhesive showed time-dependent recovery of deformation upon removal of stress, the possibility was demonstrated, with the design concept illustrated in Fig. 1, of realizing recoverable nonlinear deformation in beam structures (as exemplified in Fig. 7).

## Effect of Adhesive Properties on Beam Performance

### *Significance of Adhesive Properties*

It was demonstrated that shear connection (i.e. the adhesive layer in this study) plays a vital role in achieving the nonlinear and ductile load-deformation response through the change in composite action with loading. An adhesive with high shear modulus at relatively low stress level might provide high or full composite action at the early loading stage so that layered or composite beam structures deform with high stiffness. To realize nonlinearity and ductility in the load-deformation response in the subsequent stage, it was important that the adhesive was stressed to the nonlinear stage at a load level before ultimate failure of the beam structure. The load at which the adhesive became nonlinear also affected the ultimate load capacity of the layered beam, because a partial composite action would alter the linear strain distribution on the section and introduce higher strain and stress to the top and soffit of a beam section. Several ductile adhesives are available with different moduli, strengths, and strain capacities (Table 3). The selection of ductile adhesive should be made carefully in consideration of the structural material and cross section configuration. For the cross section in the present study, the DP8005 adhesive was used because it offered high composite action (and thus large beam stiffness) at the initial stage and plasticizes when the load increases, thus causing reduced composite action before the ultimate stage. With this adhesive, the proposed concept can be well demonstrated through the change in composite action and the associated ductile load-displacement responses. Considering the variety of ductile adhesives and the importance of their selection, the effects of different adhesives (with different moduli and strengths) on the overall beam performance were parametrically investigated using the experimentally validated FE modeling and theoretical analysis.

### *Effect of Adhesive Modulus on Beam Flexural Stiffness*

Fig. 10 shows, for a layered beam with the same dimensions as the specimens in this study, the relation between the beam stiffness $S$ (calculated as $P/\delta$) and the shear modulus $G$ of the adhesive. On the vertical axis, the beam stiffness is normalized as a stiffness ratio $S/S_c$ where $S_c$ is the stiffness when full composite action is present. Results from the layered beam theory developed by Allen (1969) are shown in Fig. 10, as well as those from the FE modeling.

From the layered beam theory (Allen 1969), under three-point bending the stiffness $S$ is calculated by

$$S = 1 \Big/ \left[\frac{L^3}{48EI} + \frac{(1 - I_f/I)^2 \psi}{4AG}\right] \tag{1}$$

where $L$ = span length; $I_f$ = sum of moment of inertias of face layers (rectangular FRP sections in this study) about their own centroidal axes; $I$ = sum of moments of inertia of FRP sections about entire section's centroidal axis; $A = bd^2/c$ = effective shear area, where $b$ = section width, $d$ = distance between the centroids of FRP sections, and $c$ = thickness of core (adhesive layer); $E$ = elastic modulus of FRP sections; $G$ = shear modulus of the adhesive, and

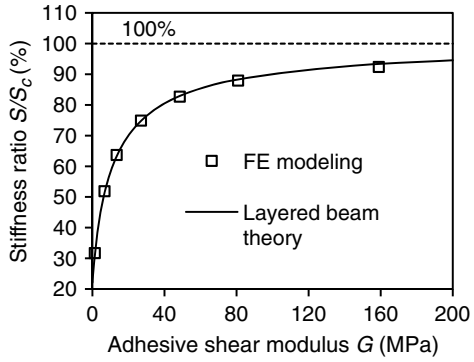


**Fig. 10.** Effect of adhesive shear modulus ($G$) on stiffness of the layered beam from layered beam theory and FE modeling ($S_c$ = stiffness when full composite action is present).

$$\psi = 1 - \frac{\sinh\theta + \beta(1-\cosh\theta)}{\theta} \tag{2}$$

where

$$\beta = \frac{\sinh\theta - (1-\cosh\theta)\tanh\phi}{\sinh\theta} \tag{3}$$

$$\theta = \frac{L}{c}\sqrt{\frac{G}{2E}\frac{c}{t}\left(1+\frac{3d^2}{t^2}\right)} \tag{4}$$

$$\phi = L_1\sqrt{\frac{AG}{EI_f(1-I_f/I)}} \tag{5}$$

where $t$ = thickness of face layer; and $L_1$ = length of overhang.

From the layered beam theory, the stiffness of full composite action ($S_c$) is calculated by Eq. (6). In the FE modeling, $S_c$ was obtained by defining the adhesive layer as the same material as the FRP

$$S_c = \frac{48EI}{L^3} \tag{6}$$

Although the layered beam theory considers shear deformation of the adhesive layer, it ignores the shear deformation of the FRP sections and flexural stiffness of the adhesive layer. Because the shear deformation of the FRP sections is negligible compared with the flexural deformation (with a span:depth ratio of 15) and the thin adhesive layer at the midsection depth contributes little to the overall section stiffness, the theoretical and FE analysis produced almost coinciding results (Fig. 10). From both the theoretical and FE results, the stiffness ratio ($S/S_c$) increased rapidly with the adhesive shear modulus ($G$) at small values, e.g. a significant change of $S/S_c$ (22%–95%) was associated with $G$ in the range of 0–200 MPa; then the ratio $S/S_c$ stabilized and converged toward 100%. The acrylic adhesive in this study (with an initial $G$ of 159 MPa) resulted in $S/S_c$ ratios of 93.3% and 92.4% according to the layered beam theory and FE modeling respectively, indicating an almost full composite action at the initial elastic stage (Fig. 10). With the epoxy adhesive used in this study (with a constant $G = 1{,}659$ MPa), full composite action was obtained, in which $S/S_c$ was 99.3% according to the layered beam theory and 98.7% according to the FE modeling. Furthermore, according to the layered beam theory, when $G$ approached 0 MPa (representing noncomposite action), the ratio $S/S_c$ converged to approximately 22%. The corresponding stiffness $S$ was approximately 0.0968 kN/mm, which is close to the average postelastic stiffness of the AM specimens (0.112 kN/mm), suggesting that little shear stiffness was offered by the adhesive layer after its elastic stage.

### *Effect of Adhesive Strength on Beam Flexural Capacity*

To study the effect of adhesive strength, different plastic strengths ($\sigma_p$) were input for the ductile acrylic adhesive in the FE modeling, whereas its elastic modulus and the linear-plastic characteristic of the stress–strain relationship were kept consistent with those in Fig. 3. The ultimate loads $P_{u,FE}$ still were governed by the tensile failure of FRP at the soffit, as in the experimental scenario. To clarify the relation between the load-displacement ($P$-$\delta$) response and the plastic strength of the adhesive ($\sigma_p$) for a larger range of the latter, different values of $\sigma_p$ were considered such that the FE specimens exhibited different levels of elastic loads ($P_{e,FE}$) and ultimate loads ($P_{u,FE}$) up to the ultimate load of the layered beam with full composite action. Fig. 11(a) shows the $P$-$\delta$ curves when different $\sigma_p$ were adopted. An increased $\sigma_p$ increased the elastic load ($P_{e,FE}$) and the ultimate load ($P_{u,FE}$) capacities of the layered beam specimen, whereas the postelastic stiffness was almost unaffected, i.e., in Fig. 11(a) the postelastic tangent lines are almost parallel regardless of different values of $\sigma_p$. The postelastic stiffness remained unchanged because of the consistent plastic behavior of the adhesive (same postelastic shear modulus) after its initial linear elasticity. Based on the results in the previous section, the postelastic stiffness of the present layered beam can range between 22% and 100% of the full composite action stiffness ($S_c$) depending on the postelastic shear modulus of the adhesive (Fig. 10). Furthermore, the postelastic stiffness of the beam can be tailored by altering the number

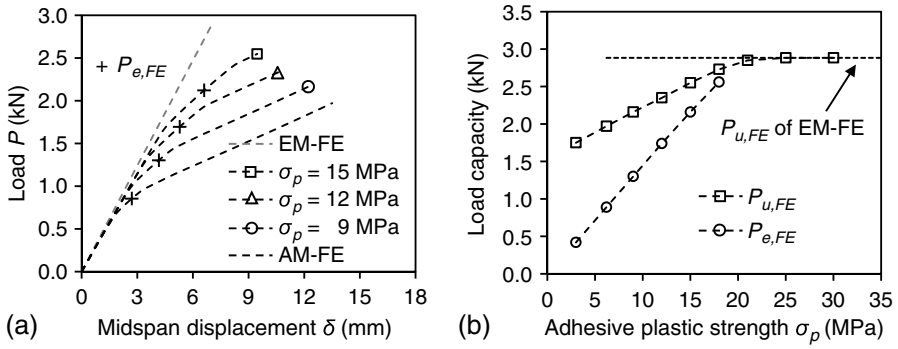


**Fig. 11.** Effect from FE modeling of adhesive plastic strength ($\sigma_p$) on (a) load-displacement ($P$-$\delta$) behavior; and (b) load capacities ($P_{e,FE}$ and $P_{u,FE}$).

of beam layers and the layer position and thickness. The increased $\sigma_p$ may compromise the nonlinear deformation and ductility of the beam specimen, because the elastic load ($P_e$) is attained at a higher displacement and the ultimate load ($P_u$) is attained at a lower displacement [Fig. 11(a)].

Fig. 11(b) presents the relation between the load capacities of the layered beam ($P_{e,FE}$ and $P_{u,FE}$) and the plastic strength of the ductile adhesive ($\sigma_p$). Governed directly by the adhesive plastic strength ($\sigma_p$), the elastic load ($P_{e,FE}$) increases almost linearly with $\sigma_p$. It would extend to the origin point ($P_{e,FE} = 0$ kN) at $\sigma_p = 0$ MPa (and shear modulus $G = 0$ MPa), because there is no composite action between the two FRP sections all along the loading process in this case. This linearly ascending curve between $P_{e,FE}$ and $\sigma_p$ ends when the value of $P_{e,FE}$ converges to that of $P_{u,FE}$, indicating that the elastic capacity is preceded by the ultimate capacity governed by the material failure of the FRP in this case. The ultimate load capacity $P_{u,FE}$, although governed by the material failure of the FRP, also increased with $\sigma_p$ [Fig. 11(b)]. This is because greater adhesive plastic strength delays the occurrence of partial composite action (thereby delaying the onset of nonlinear strain distribution along the section depth), which introduces higher strain peaks at the outermost fibers. The linearly ascending $P_{u,FE}$–$\sigma_p$ curve shows an intercept of 1.54 kN at $\sigma_p$ of 0 MPa [Fig. 11(b)], suggesting the load capacity of the beam when the two FRP sections act separately, i.e. without composite action between the two sections. In this case of noncomposite action, the load capacity of 1.54 kN is close to the sum of the capacities of two individual FRP sections (0.73 kN for each section from FE modeling) and about half the load capacity of the EM specimen ($P_{u,FE} = 2.88$ kN) with full composite action ($S/S_c = 98.7\%$). This relation exists because, theoretically, two halved section depths ($h$) result in a halved section modulus ($S = bh^2/6$). Furthermore, beyond $\sigma_p$ of around 20 MPa, the curve of $P_{u,FE}$ stopped increasing because the initial high composite action ($S/S_c = 92.4\%$) can be maintained all the way to the ultimate load capacity governed by the tensile failure of the FRP [Fig. 11(b)].

The relations between beam performance and the adhesive properties discussed suggest that the nonlinear load-deformation response of the layered beam can be tailored by selection of ductile adhesives with different moduli and strengths. The layered beams of the present configuration were examined in the experimental program and parametric studies to focus on the load-dependent composite action and the associated effects from the adhesive properties. This structural concept may be applied to other geometric configurations and linear elastic and brittle materials, but careful design should be exercised regarding more-complex structural responses and various failure modes other than the targeted load-dependent composite action. For example, possible structural failure may occur before the decrease of composite action, and this may not be desirable for realization of ductile structural responses through this concept. The quality of adhesive bonding also needs to be ensured for application of the proposed approach at large scale, and a few previous researchers have shown successful examples of large-scale application of adhesive bonding (Hejll et al. 2005; Singamsethi et al. 2005; Shi et al. 2017). The FE modeling approach demonstrated in this study can aid in the selection of appropriate adhesive properties and evaluation of the beam performance when other geometric configurations are considered.

## Example Demonstration for Practice

To demonstrate the applicability of the proposed concept in engineering structures, numerical investigation was conducted to evaluate the performance of a beam structure with a built-up section in which the concept of load-dependent composite action was applied. The built-up section in this investigation [Fig. 12(a)] consisted of two GFRP box sections ($50 \times 50 \times 8$ mm) bonded together. Again, both Sikadur-330 and DP8005 adhesives were used, and typical material properties of pultruded GFRP were considered (Hollaway 2010) [Fig. 12(a)]. Two realistic loading scenarios, one with a midspan point load $P$ (Scenario 1) and the other with a uniformly distributed load $Q$ (Scenario 2), were examined for a span of 1,300 mm as an example under a simply supported boundary condition [Fig. 12(b)] to investigate the overall beam performance. The ultimate failure of the beam structures was evaluated against tensile and compressive failure at the top or soffit of the section, or the shear failure of the webs.

The load-displacement responses of the built-up beams are plotted in Fig. 13. Under the midspan point load $P$ (Scenario 1), the ultimate stage was attained by the tensile failure of GFRP at the midspan soffit. Under the uniformly distributed load $Q$ (Scenario 2), the ultimate failure occurred as web shear failure near the end support location. In both load scenarios, the design with the ductile adhesive DP8005 provided nonlinear and ductile load-displacement responses with major stiffness reductions at an elastic load level of 28 kN or 37 kN/m, after the plasticization of the shear connection (adhesive layer) with the associated reduction in composite action. Compared with the design with the linear elastic adhesive, the beam with a ductile adhesive in Scenario 1 had 2% lower initial stiffness, 13% lower ultimate load, but 61% higher ultimate displacement [Figs. 13(a)]. For Scenario 2, with a

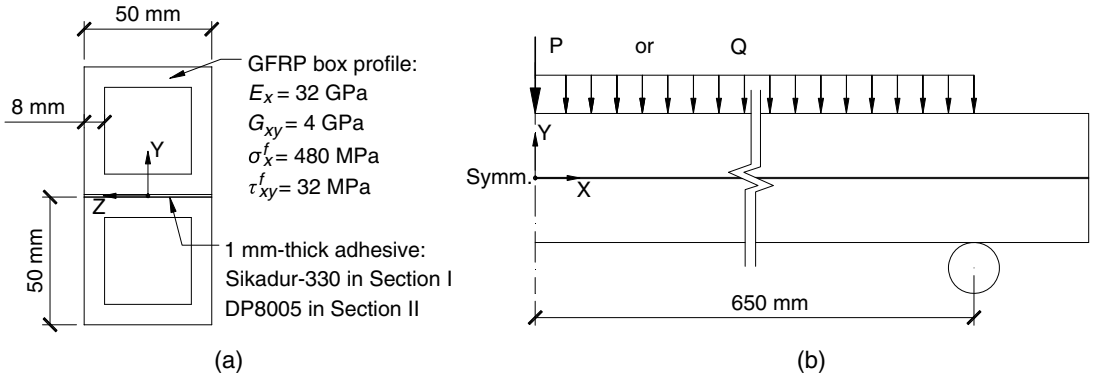


**Fig. 12.** GFRP built-up section beams: (a) cross-section dimensions and material properties ($E$ = elastic modulus, $G$ = shear modulus, $\sigma^f$ = tensile/compressive strength, and $\tau^f$ = shear strength); and (b) span dimension and load scenarios.

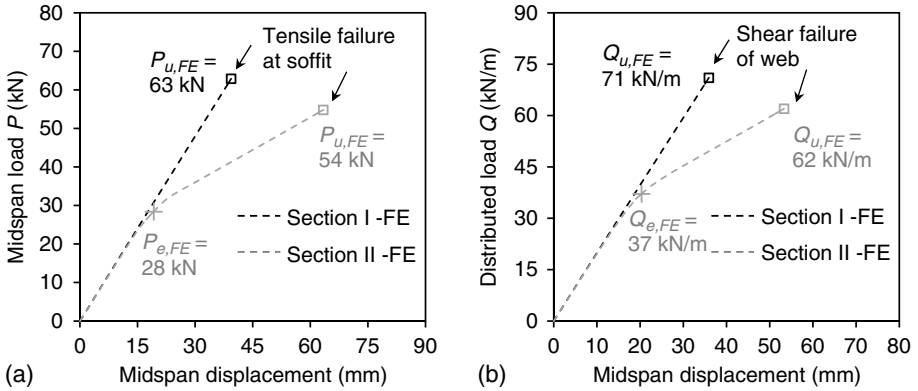


**Fig. 13.** Load-displacement responses of the GFRP built-up section beams under (a) midspan point load $P$; and (b) uniformly distributed load $Q$ (refer to Fig. 12 for cross section and span dimensions).



uniformly distributed load, the beam with ductile adhesive had 3% lower initial stiffness, 14% lower ultimate load, but 48% higher ultimate displacement [Figs. 13(b)]. Without much compromise in the initial stiffness and ultimate load capacity, the ductile performance provided by load-dependent composite action demonstrated its successful application for the design of large-scale built-up beam structures made from linear elastic and brittle materials. Similarly, this concept also may find applications in other structural forms such as sandwich structures (Manalo et al. 2010; Keller et al. 2014; Satasivam et al. 2014), composite beams (Nordin and Täljsten 2004; Correia et al. 2007), or other built-up section beams (Hejll et al. 2005; Bai et al. 2013).

## Conclusions

A structural concept was proposed to realize nonlinear and ductile load-deformation responses in beam structures of linear elastic and brittle materials. The concept uses the load-dependent composite action resulting from the nonlinear behavior of the shear connection in a layered beam. Experimental demonstration and FE modeling were conducted on layered beam specimens composed of two brittle FRP components using structural adhesive as a shear connection. The comparative study was further developed based on a linear elastic (brittle) adhesive and a nonlinear (ductile) adhesive. From these investigations, the following key findings are summarized:

1. The layered beam specimens with a linear elastic epoxy adhesive exhibited a linear load-displacement response up to failure, whereas the specimens with a nonlinear ductile acrylic adhesive successfully realized a bilinear load-displacement response because of the change in the shear modulus of the adhesive (shear connection) and the associated decrease in composite action with loading. The ultimate failure of all specimens occurred as tensile fracture of the FRP at the soffit. Compared with the specimens with epoxy adhesive, those with acrylic adhesive had 12% lower initial stiffness and 28% lower ultimate load, but 61% higher displacement capacity.
2. Under the load–unload–reload cycles, the specimens with epoxy adhesive exhibited linear unloading and reloading load-displacement paths that coincided with the initial loading path. In the specimens with acrylic adhesive, unloading from beyond the elastic load produced nonlinear paths that ended with residual deformations. After removal of the load, recovery of the residual deformation advanced rapidly within the first 20 min and then developed at a decreasing rate and stabilized at about 80% of the initial residual displacement. The subsequent reloading process produced nonlinear curves that followed the slope and nonlinearity of the initial loading curves.
3. The strain measurements confirmed that the nonlinear load-displacement behavior stemmed from the load-dependent composite action in the layered beams. As evidenced in the specimens with acrylic adhesive, loading beyond the elastic load introduced deviation of the strain distribution along the section depth from the initial linearity at the elastic stage. Such nonlinear strain distributions, together with the shear slip between the layered components, indicated a reduction in the degree of composite action with loading. The initial high composite action became a partial action because the nonlinear adhesive, acting as shear connection, decreased in shear modulus.
4. The FE modeling was capable of accurately describing the nonlinear load-displacement response of the specimens with acrylic adhesive and the development of strain distribution along the section depth. Parametric studies using the layered beam theory and FE modeling revealed that the stiffness of the layered beam decreased nonlinearly with the reduction in the shear modulus of the adhesive, suggesting, for a given cross section, a certain range of adhesive shear modulus for effective manipulation of composite action and thus beam stiffness.
5. The FE modeling also showed that the elastic load capacity increased linearly with the adhesive plastic strength until preceded by the ultimate load governed by the material failure of the FRP. The ultimate load also exhibited a linear increase with the adhesive plastic strength because a greater value of the latter delayed the occurrence of partial composite action, which accordingly introduced higher strain peaks on the section. The increase in the ultimate load with the adhesive plastic strength continued until a plateau was reached, at which the initial high composite action could be maintained and continued up to the ultimate material failure.

Further FE modeling was conducted to demonstrate the successful application of the concept in a built-up section beam structure to provide ductile performance. By a similar mechanism, the concept may be applied to other structural forms such as sandwich structures, composite beams, or other built-up section beams.

## Acknowledgments

The authors acknowledge support from the Australian Research Council through the Discovery project (DP180102208). Thanks are extended to the staffs of the Civil Engineering Laboratory

of Monash University for their assistance in the experimental program.

## References


Allen, H. G. 1969. "Sandwich beams." Chap. 2 in *Analysis and design of structural sandwich panels*. Oxford, UK: Pergamon.

Amada, S., Y. Ichikawa, T. Munekata, Y. Nagase, and H. Shimizu. 1997. "Fiber texture and mechanical graded structure of bamboo." *Compos. Part B* 28 (1–2): 13–20. https://doi.org/10.1016/S1359-8368(96)00020-0.

ASTM. 2014. *Standard test method for tensile properties of polymer matrix composite materials*. ASTM D3039. West Conshohocken, PA: ASTM.

Bai, Y., T. Keller, and C. Wu. 2013. "Pre-buckling and post-buckling failure at web-flange junction of pultruded GFRP beams." *Mater. Struct.* 46 (7): 1143–1154. https://doi.org/10.1617/s11527-012-9960-9.

Bai, Y., and C. Zhang. 2012. "Capacity of nonlinear large deformation for trusses assembled by brittle FRP composites." *Compos. Struct.* 94 (11): 3347–3353. https://doi.org/10.1016/j.compstruct.2012.05.016.

Banea, M., and L. F. da Silva. 2010. "The effect of temperature on the mechanical properties of adhesives for the automotive industry." *Proc. Inst. Mech. Eng. Part L: J. Mater.: Des. Appl.* 224 (2): 51–62. https://doi.org/10.1243/14644207JMDA283.

Bank, L. C. 2012. "Progressive failure and ductility of FRP composites for construction." *J. Compos. Constr.* 17 (3): 406–419. https://doi.org/10.1061/(ASCE)CC.1943-5614.0000355.

Chambers, R. E. 1997. "ASCE design standard for pultruded fiber-reinforced-plastic (FRP) structures." *J. Compos. Constr.* 1 (1): 26–38. https://doi.org/10.1061/(ASCE)1090-0268(1997)1:1(26).

Chapman, J., and S. Balakrishnan. 1964. "Experiments on composite beams." *Struct. Eng.* 42 (11): 369–383.

Clouston, P., L. A. Bathon, and A. Schreyer. 2005. "Shear and bending performance of a novel wood–concrete composite system." *J. Struct. Eng.* 131 (9): 1404–1412. https://doi.org/10.1061/(ASCE)0733-9445(2005)131:9(1404).

Correia, J. R., F. A. Branco, and J. G. Ferreira. 2007. "Flexural behaviour of GFRP–concrete hybrid beams with interconnection slip." *Compos. Struct.* 77 (1): 66–78. https://doi.org/10.1016/j.compstruct.2005.06.003.

Culver, C., and R. Coston. 1961. "Tests of composite beams with stud shear connectors." *J. Struct. Div.* 87 (2): 1–20.

da Silva, L. F., G. Critchlow, and M. Figueiredo. 2008. "Parametric study of adhesively bonded single lap joints by the Taguchi method." *J. Adhes. Sci. Technol.* 22 (13): 1477–1494. https://doi.org/10.1163/156856108X309585.

da Silva, L. F., T. Rodrigues, M. Figueiredo, M. De Moura, and J. Chousal. 2006. "Effect of adhesive type and thickness on the lap shear strength." *J. Adhes.* 82 (11): 1091–1115. https://doi.org/10.1080/00218460600948511.

de Castro, J., and T. Keller. 2008. "Ductile double-lap joints from brittle GFRP laminates and ductile adhesives, Part I: Experimental investigation." *Compos. Part B* 39 (2): 271–281. https://doi.org/10.1016/j.compositesb.2007.02.015.

Dodoo, A., L. Gustavsson, and R. Sathre. 2014. "Lifecycle primary energy analysis of low-energy timber building systems for multi-storey residential buildings." *Energy Build.* 81 (Oct): 84–97. https://doi.org/10.1016/j.enbuild.2014.06.003.

Faella, C., E. Martinelli, and E. Nigro. 2003. "Shear connection nonlinearity and deflections of steel–concrete composite beams: A simplified method." *J. Struct. Eng.* 129 (1): 12–20. https://doi.org/10.1061/(ASCE)0733-9445(2003)129:1(12).

Gai, X., A. Darby, T. Ibell, and M. Evernden. 2013. "Experimental investigation into a ductile FRP stay-in-place formwork system for concrete slabs." *Constr. Build. Mater.* 49 (Dec): 1013–1023. https://doi.org/10.1016/j.conbuildmat.2012.08.050.

Hejll, A., B. Täljsten, and M. Motavalli. 2005. "Large scale hybrid FRP composite girders for use in bridge structures—theory, test and field application." *Compos. Part B* 36 (8): 573–585. https://doi.org/10.1016/j.compositesb.2005.05.002.

Hollaway, L. 2010. "A review of the present and future utilisation of FRP composites in the civil infrastructure with reference to their important in-service properties." *Constr. Build. Mater.* 24 (12): 2419–2445. https://doi.org/10.1016/j.conbuildmat.2010.04.062.

Jayas, B., and M. Hosain. 1988. "Behaviour of headed studs in composite beams: Push-out tests." *Can. J. Civ. Eng.* 15 (2): 240–253. https://doi.org/10.1139/l88-032.

Keller, T., and J. de Castro. 2005. "System ductility and redundancy of FRP beam structures with ductile adhesive joints." *Compos. Part B* 36 (8): 586–596. https://doi.org/10.1016/j.compositesb.2005.05.001.

Keller, T., and H. Gürtler. 2005. "Quasi-static and fatigue performance of a cellular FRP bridge deck adhesively bonded to steel girders." *Compos. Struct.* 70 (4): 484–496. https://doi.org/10.1016/j.compstruct.2004.09.028.

Keller, T., J. Rothe, J. De Castro, and M. Osei-Antwi. 2014. "GFRP-balsa sandwich bridge deck: Concept, design, and experimental validation." *J. Compos. Constr.* 18 (2): 04013043. https://doi.org/10.1061/(ASCE)CC.1943-5614.0000423.

Keller, T., E. Schaumann, and T. Vallée. 2007. "Flexural behavior of a hybrid FRP and lightweight concrete sandwich bridge deck." *Compos. Part A* 38 (3): 879–889. https://doi.org/10.1016/j.compositesa.2006.07.007.

Lee, S., M. Munro, and R. Scott. 1990. "Evaluation of three in-plane shear test methods for advanced composite materials." *Composite* 21 (6): 495–502. https://doi.org/10.1016/0010-4361(90)90422-S.

Liese, W. 1987. "Research on bamboo." *Wood Sci. Technol.* 21 (Sep): 189–209. https://doi.org/10.1007/BF00351391.

Machado, J., P.-R. Gamarra, E. Marques, and L. F. da Silva. 2018. "Improvement in impact strength of composite joints for the automotive industry." *Compos. Part B* 138 (Apr): 243–255. https://doi.org/10.1016/j.compositesb.2017.11.038.

Manalo, A., T. Aravinthan, and W. Karunasena. 2010. "Flexural behaviour of glue-laminated fibre composite sandwich beams." *Compos. Struct.* 92 (11): 2703–2711. https://doi.org/10.1016/j.compstruct.2010.03.006.

Meier, U., T. Triantafillou, and N. Deskovic. 1995. "Innovative design of FRP combined with concrete: Short-term behaviour." *J. Struct. Eng.* 121 (7): 1069–1078. https://doi.org/10.1061/(ASCE)0733-9445(1995)121:7(1069).

Nie, J., and C. S. Cai. 2003. "Steel–concrete composite beams considering shear slip effects." *J. Struct. Eng.* 129 (4): 495–506. https://doi.org/10.1061/(ASCE)0733-9445(2003)129:4(495).

Nie, J., J. Fan, and C. Cai. 2008. "Experimental study of partially shear-connected composite beams with profiled sheeting." *Eng. Struct.* 30 (1): 1–12. https://doi.org/10.1016/j.engstruct.2007.02.016.

Nordin, H., and B. Täljsten. 2004. "Testing of hybrid FRP composite beams in bending." *Compos. Part B* 35 (1): 27–33. https://doi.org/10.1016/j.compositesb.2003.08.010.

Oehlers, D., P. Visintin, M. Haskett, and W. Sebastian. 2013. "Flexural ductility fundamental mechanisms governing all RC members in particular FRP RC." *Constr. Build. Mater.* 49 (Dec): 985–997. https://doi.org/10.1016/j.conbuildmat.2013.02.018.

Pinto, A. M. G., A. Magalhães, R. D. S. G. Campilho, M. De Moura, and A. Baptista. 2009. "Single-lap joints of similar and dissimilar adherends bonded with an acrylic adhesive." *J. Adhes.* 85 (6): 351–376. https://doi.org/10.1080/00218460902880313.

Porteous, J., and A. Kermani. 2013. *Structural timber design to Eurocode 5*. New York: Wiley.

Qiu, C., Y. Bai, L. Zhang, and L. Jin. 2019. "Bending performance of splice connections for assembly of tubular section FRP members: Experimental and numerical study." *J. Compos. Constr.* 23 (5): 04019040. https://doi.org/10.1061/(ASCE)CC.1943-5614.0000964.

Qiu, C., C. Ding, X. He, L. Zhang, and Y. Bai. 2018. "Axial performance of steel splice connection for tubular FRP column members." *Compos. Struct.* 189 (Apr): 498–509. https://doi.org/10.1016/j.compstruct.2018.01.100.

Queiroz, F., P. Vellasco, and D. Nethercot. 2007. "Finite element modelling of composite beams with full and partial shear connection." *J. Constr. Steel Res.* 63 (4): 505–521. https://doi.org/10.1016/j.jcsr.2006.06.003.

Quinson, R., J. Perez, M. Rink, and A. Pavan. 1997. "Yield criteria for amorphous glassy polymers." *J. Mater. Sci.* 32 (5): 1371–1379. https://doi.org/10.1023/A:1018525127466.

Salari, M. R., E. Spacone, P. B. Shing, and D. M. Frangopol. 1998. "Nonlinear analysis of composite beams with deformable shear connectors." *J. Struct. Eng.* 124 (10): 1148–1158. https://doi.org/10.1061/(ASCE)0733-9445(1998)124:10(1148).

Satasivam, S., and Y. Bai. 2016. "Mechanical performance of modular FRP-steel composite beams for building construction." *Mater. Struct.* 49 (10): 4113–4129. https://doi.org/10.1617/s11527-015-0776-2.

Satasivam, S., Y. Bai, and X.-L. Zhao. 2014. "Adhesively bonded modular GFRP web–flange sandwich for building floor construction." *Compos. Struct.* 111 (May): 381–392. https://doi.org/10.1016/j.compstruct.2014.01.003.

Satasivam, S., P. Feng, Y. Bai, and C. Caprani. 2017. "Composite actions within steel-FRP composite beam systems with novel blind bolt shear connections." *Eng. Struct.* 138 (May): 63–73. https://doi.org/10.1016/j.engstruct.2017.01.068.

Shi, H., W. Liu, H. Fang, Y. Bai, and D. Hui. 2017. "Flexural responses and pseudo-ductile performance of lattice-web reinforced GFRP-wood sandwich beams." *Compos. Part B* 108 (Jan): 364–376. https://doi.org/10.1016/j.compositesb.2016.10.009.

Singamsethi, S., J. LaFave, and K. Hjelmstad. 2005. "Fabrication and testing of cuff connections for GFRP box sections." *J. Compos. Constr.* 9 (6): 536–544. https://doi.org/10.1061/(ASCE)1090-0268(2005)9:6(536).

Steinberg, E., R. Selle, and T. Faust. 2003. "Connectors for timber–lightweight concrete composite structures." *J. Struct. Eng.* 129 (11): 1538–1545. https://doi.org/10.1061/(ASCE)0733-9445(2003)129:11(1538).

Tomasi, R., M. A. Parisi, and M. Piazza. 2009. "Ductile design of glued-laminated timber beams." *Pract. Period. Struct. Des. Constr.* 14 (3): 113–122. https://doi.org/10.1061/(ASCE)1084-0680(2009)14:3(113).

Wang, Y. 1998. "Deflection of steel-concrete composite beams with partial shear interaction." *J. Struct. Eng.* 124 (10): 1159–1165. https://doi.org/10.1061/(ASCE)0733-9445(1998)124:10(1159).

Ward, I. M. 1971. "The yield behaviour of polymers." *J. Mater. Sci.* 6 (11): 1397–1417. https://doi.org/10.1007/BF00549685.

Yang, X., Y. Bai, and F. Ding. 2015. "Structural performance of a large-scale space frame assembled using pultruded GFRP composites." *Compos. Struct.* 133 (Dec): 986–996. https://doi.org/10.1016/j.compstruct.2015.07.120.

Yang, X., Y. Bai, F. J. Luo, X.-L. Zhao, and F. Ding. 2016. "Dynamic and fatigue performances of a large-scale space frame assembled using pultruded GFRP composites." *Compos. Struct.* 138 (Mar): 227–236. https://doi.org/10.1016/j.compstruct.2015.11.064.

Zhang, Z. J., Y. Bai, and X. Xiao. 2018. "Bonded sleeve connections for joining tubular glass fiber–reinforced polymer beams and columns: Experimental and numerical studies." *J. Compos. Constr.* 22 (4): 04018019. https://doi.org/10.1061/(ASCE)CC.1943-5614.0000853.